A Simplified and Versatile Element Model for Elastomeric Seismic Isolation Bearings

Sebastián Miranda,[a), c)] M.EERI, **Eduardo Miranda,**[b)] M.EERI and **Juan Carlos de la Llera,**[a)] M.EERI.

A novel approach for two-dimensional modeling of elastomeric bearings using three springs in parallel is presented. This simplified element model considers: i) an elastoplastic spring with a smooth transition between branches; ii) a linear elastic spring; and iii) a non-linear elastic spring, and is fully defined by only six parameters. The main advantages of the simplified model are twofold: 1) Versatility, as a single model is capable of accurately reproduce the main characteristics of the hysteretic behavior of different types of rubber-based seismic isolators, including low damping rubber bearings (LDRBs), high damping rubber bearings (HDRBs), and lead - core rubber bearings (LRBs); and 2) Simplicity, as it requires fewer parameters and it is easier to calibrate from experimental cyclic tests results than most currently available models. Model parameters identification is illustrated using quasi-static cyclic and earthquake simulator tests of HDRBs and LRBs, demonstrating that the model shows a good agreement between the test-measured and model-predicted hysteretic behavior. Different objective functions are evaluated in the optimization procedure, and their effect on the identified parameters is studied and discussed. This practitioner-oriented model is particularly amenable for implementation in general-purpose structural analysis software. Its usage is strongly recommended as an initial-stage design tool to select the optimal isolation system for a specific project.

INTRODUCTION

Seismic isolation has shown to be one of the most effective and sometimes economical seismic protection technology. In particular, it is one of the few protection systems that, when

[a)] National Research Center for Integrated Natural Disaster Management, CONICYT/FONDAP/15110017, Faculty of Engineering, Pontificia Universidad Católica de Chile, Chile
[b)] John A. Blume Earthquake Engineering Center, Department of Civil and Environmental Engineering, Stanford University, Stanford, CA 94305-4020, U.S.A.
[c)] Faculty of Engineering, Universidad del Desarrollo, Santiago, Chile

adequately implemented, can simultaneously achieve significant reductions in interstory drift demands, horizontal accelerations, and lateral forces in buildings. For the selection of the type of bearing as well as for its characteristics that will result in an adequate control of lateral force and deformation demands in the superstructure, it is necessary to explicitly model their cyclic behavior. In particular, in the context of applications in engineering practice, the words of George E. Box resonate (Box et al., 2011): “all models are wrong, but some models are useful.” In the second edition of his book, the author added that the question to ask was not if the model is exact (it never is) but just if the model is good enough to produce useful results for a particular application.

Among the different types of seismic isolators, the ones manufactured from high damping rubber (HDRBs) and the ones with a lead-core in their center (LRBs) have a strongly non-linear force-displacement relationship, especially at large lateral shear strains where alignment of polymeric chains and crystallization in the rubber make the material considerably stiffer. Additionally, these types of isolators have several other well-known characteristics such as: (i) Mullins effect (Mullins 1969) that produces degradation of the peak lateral force and lateral stiffness when the isolation bearing is subjected to cyclic loading; (ii) axial load dependency; (iii) strain-rate dependency; (iv) load-path dependency; and (v) internal temperature dependency.

Kikuchi and Aiken (1997) provided a summary of several early models for elastomeric rubber bearings. Typically, a Ramberg-Osgood (Ramberg and Osgood 1943) or a bilinear constitutive model were used. However, to adequately model the behavior of the isolators, the bearing parameters need to be updated as a function of shear strain. Furthermore, Kikuchi and Aiken noted that the Ramberg-Osgood model was suitable for low-to-moderate shear strains, but it did not capture the stiffening effect on rubber-based isolators subjected to large shear strains. Other modeling approaches have implemented the Ozdemir (Ozdemir 1976) or the Wen (Wen 1976) constitutive relationships that use a differential equation to track the isolator's current state. Hence, in these cases, the model parameters do not need to be updated.

After assessing the accuracy of several formulations available to that date, Kikuchi and Aiken (1997) proposed a new set of equations, characterizing the force in the isolator as a function of shear strain. The Kikuchi and Aiken model, which does not consider differential equations for tracking the isolator current state, showed a much better agreement with the experimental data than many other models, especially if hardening effects were present in the high shear strain range. The Kikuchi and Aiken model requires the calibration of seven parameters, not constants but defined as isolator shear strain functions, and considers a simplified procedure to incorporate stiffness degradation that occurs as the deformation cycles evolve.

Pang and Yang (1996) proposed a model that explicitly splits the isolator force between a restoring component and a viscoelastic damping component, both non-linear functions of the isolator displacement and velocity. Hwang et al. (2002) improved the Pang and Yang (1996) model by including the degradation of the stiffness and the dissipated energy as the deformation cycles evolve. They also simplified the model mathematical formulation as the number of parameters to calibrate was reduced from eleven to ten.

Tsai et al. (2003) recognized that the second generation of models, including the Kikuchi and Aiken (1997) model, effectively included the stiffening effect, but there was still the necessity of more straightforward approaches including, for example, the HDRBs strain rate-dependency. The authors proposed a model based on the Bouc-Wen (Wen 1976) constitutive model, modified to include this effect.

Abe et al. (2004) proposed a model capable of considering multiaxial loading, based on the Ozdemir (Ozdemir 1976) elastoplastic model, that also uses differential equations for tracking the state of the system. The Abe et al. model also includes an isotropic hardening displacement-dependent term and a non-linear elastic spring. The one-dimensional version of this model requires the calibration of thirteen parameters. The differential equation approach in this type of models has proven to considerably restrict their implementation in engineering design procedures. Table 1 shows a summary of several models and their main features.

All models listed in Table 1 consider, with different approaches, the significant isolator hardening effect at large shear strains. Additionally, some of them include highly complex phenomena as the strain-rate dependency or the stress softening behavior. However, the influence of these phenomena in the seismic response of isolated structures is still being investigated. In a recent work by Tubaldi et al. (2017), a new model, especially suited for the stress softening effect assessment, was developed. Its implementation on an SDOF system suggested that using a simplified fully-scragged condition in seismic isolation modeling leads to a low to moderate overestimation of the displacements under typical seismic conditions. On the other hand, under near-fault seismic conditions, simulations based on a fully scragged condition could lead to nonrealistic large displacements.

Table 1. Summary of the most frequently used models.

Model	Calibration parameters	Displacement dependency	Differential Equation	Main Features
Tsopelas et al. (1994)	6	No	Yes	• Biaxial behavior • Does not consider cyclic softening effect.
Pan and Yang (1996)	11	No	No	• Uniaxial behavior • Does not consider cyclic softening effect.
Kikuchi and Aiken (1997)	7	Yes	No	• Uniaxial behavior • Considers cyclic softening effect.
Hwang et al. (2002)	10	No	No	• Uniaxial behavior • Considers cyclic softening effect.
Tsai et al. (2003)	7	No	Yes	• Biaxial behavior • Considers rate-dependency effects.
Abe et al. (2004)	13	No	Yes	• Biaxial behavior • Considers isotropic hardening.

Table 1 shows that most of the existing models require a large number of parameters, which are often hard to calibrate, especially in models in which these parameters are not constants, but functions that depend on the shear strain in the isolator. Most of these models are research-oriented, and therefore have not been implemented in commercially available structural analysis programs nor they are used in practice for evaluating the seismic response of isolated structures. On the other hand, most seismic regulatory codes prescribe quite simplified design methodologies based on an equivalent linearization of the isolators' force-displacement relationship or just refer to bilinear models. These approaches neglect features as high shear-strain hardening and may not lead to an adequate estimate of lateral forces, displacements, and accelerations on the structure.

The proposed simplified model aims to capture the main features of the behavior of elastomeric rubber bearings (ERB), especially the high shear-strain hardening, using a significantly simpler mathematical formulation that requires fewer easier-to-calibrate parameters than other models available in the literature. Although the model is aimed at ERB, it converges easily to the frequently-used kinematic-hardening bilinear model, so it can also be used to approximately represent the behavior of single and double curvature curved-surface sliding (CSS) isolation bearings. Based on the features described above, this model can be efficiently used to: i) select the most suitable isolator type for a specific project in the early stages of the design process (e.g., ERB or CSS), ii) assess the relevance of high shear-strain hardening in already implemented rubber-based isolation systems that were designed using equivalent linearization or bilinear modeling, through a deterministic approach, iii) evaluate, using the Performance-Based Earthquake Engineering (PBEE) framework, the performance of currently installed elastomeric isolators, particularly in applications where the seismic hazard has been updated, or special concerns over isolator safety apply, and iv) estimate with higher accuracy the lateral forces, displacements and accelerations demands in new structures protected with rubber-based devices.

The main objectives of this research are: (1) to propose a simplified and versatile practitioner-oriented model, able to capture relevant features of the behavior of elastomeric seismic isolators that currently are not considered by the standard design procedures; (2) to demonstrate that the model is capable of representing with reasonable accuracy the measured behavior of different types of elastomeric seismic isolators when subjected to quasi-static cyclic loading and earthquake simulation tests; (3) to study if the parameters that define the model need to be defined as a function of the isolator shear strain or could be defined as constants; (4) to identify the model parameters using system identification techniques combined with different objective functions minimizing error in dissipated energy, force history, and stiffness history during a deformation cycle; and (5) to study the sensitivity of the model-predicted response to the objective function used to perform the parameter calibration.

ANALYTICAL MODEL

The simplified model is based on several aspects of the Kikuchi-Aiken model but makes several modifications that make it more versatile and easier to calibrate. Like the Kikuchi-Aiken model, the proposed model is based on springs arranged in parallel. The three springs that define this simplified model are shown in Figure 1. One of them has a hysteretic behavior based on the well-known Menegotto-Pinto model (Menegotto and Pinto 1973) initially developed for modeling steel reinforcing bars in reinforced concrete. The Menegotto-Pinto model is characterized by four parameters: (i) F_y, the yield force; (ii) u_y, the yield displacement; (iii) R, a parameter that controls the shape of the transition between the elastic and the plastic branches; and (iv) b the ratio of the secondary to initial stiffness. In steel modeling, the R parameter represents the Bauschinger effect (Bauschinger, 1881), and its value is typically a function of the maximum inelastic displacement experienced by the steel specimen.

The Menegotto-Pinto model can be easily interpreted as two springs acting in parallel, namely $F_1(u)$ and $F_2(u)$, where F_1 and F_2 are the forces acting in each spring, and u is the displacement. As can be seen in Figure 2, $F_1(u)$ is an elastoplastic spring with a smooth transition between its branches, and $F_2(u)$ is a linear elastic spring.

To include the hardening effect that characterizes isolators' response when subjected to moderate and high levels of lateral shear strain, a non-linear elastic spring, namely $F_3(u)$, is included. This non-linear spring is defined by two parameters: (i) F_o, the force associated with the hardening displacement u_h; and (2) n, a parameter that controls the nonlinearity of the spring. By adding the contributions of the three springs in the simplified model, the complete equation giving the force as a function of the displacement is:

$$F(u) = F_1(u) + F_2(u) + F_3(u) \qquad (1)$$

$$F(u) = \frac{\frac{F_y}{u_y}(1-b)u}{\left(1+\left(\frac{u}{u_y}\right)^R\right)^{\frac{1}{R}}} + \frac{F_y}{u_y}bu + F_o\, sign(u)\left(\frac{|u|}{u_h}\right)^n \qquad (2)$$

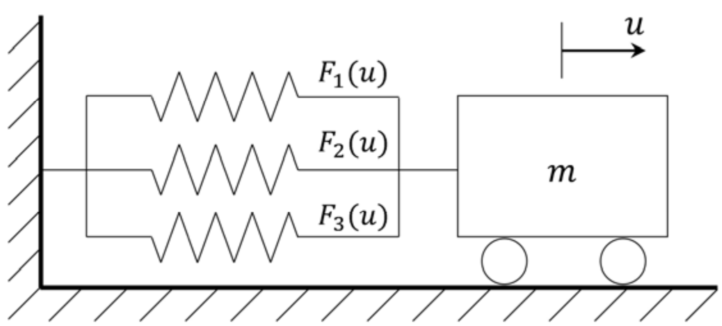

Figure 1. Proposed analytical model.

Figure 2 shows plots of force as a function of displacement for the three springs in the simplified model. A comparison between the original Menegotto-Pinto model and the proposed model incorporating $F_3(u)$ to account for hardening effects is shown in Figure 3.

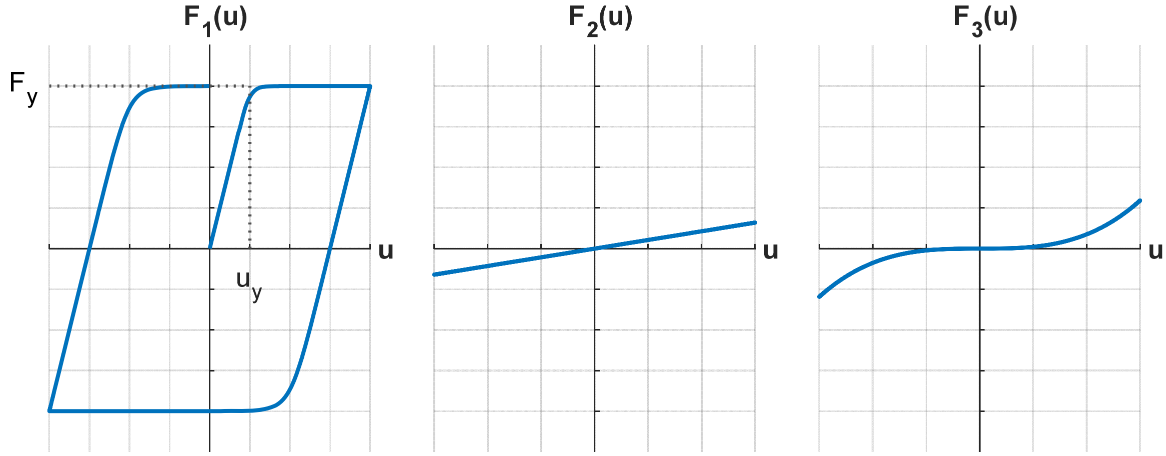

Figure 2. Force as a function of displacement for the three springs in the model.

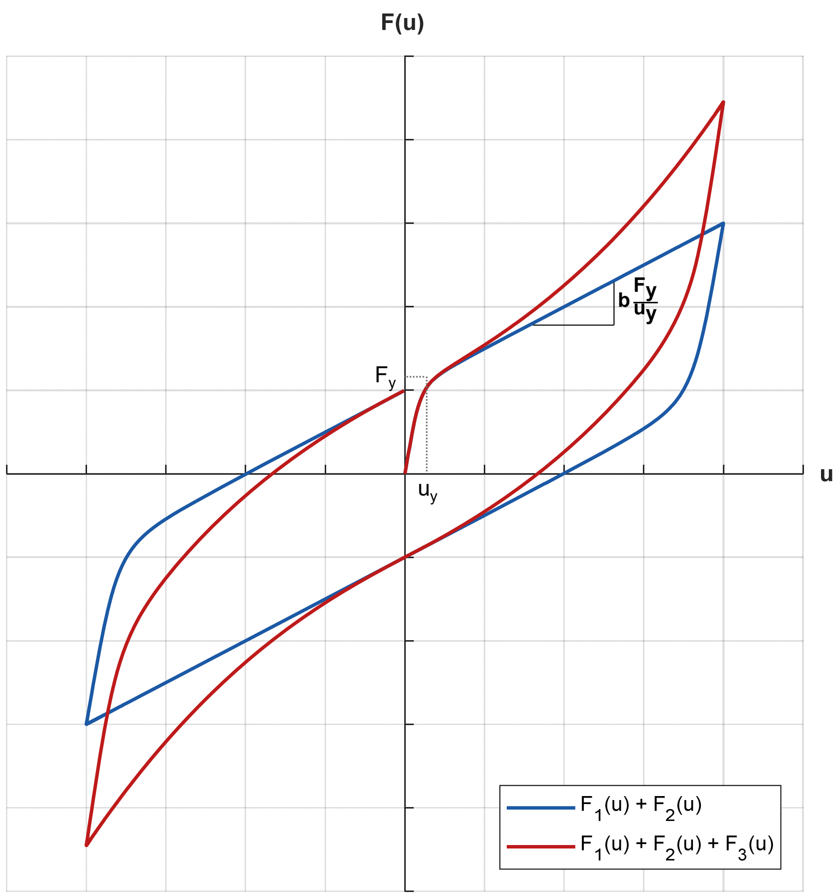

Figure 3. Force as a function of displacement for: a) $F_1(u) + F_2(u)$, the original Menegotto-Pinto Model, and b) $F_1(u) + F_2(u) + F_3(u)$, the model proposed in this work.

The parameters defining the springs $F_1(u)$ and $F_3(u)$ and the overall effect of their variation on the springs force-displacement constitutive relations are displayed in Figures 4 and 5, respectively. For the $F_1(u)$ spring case, the plots consider $b = 0$.

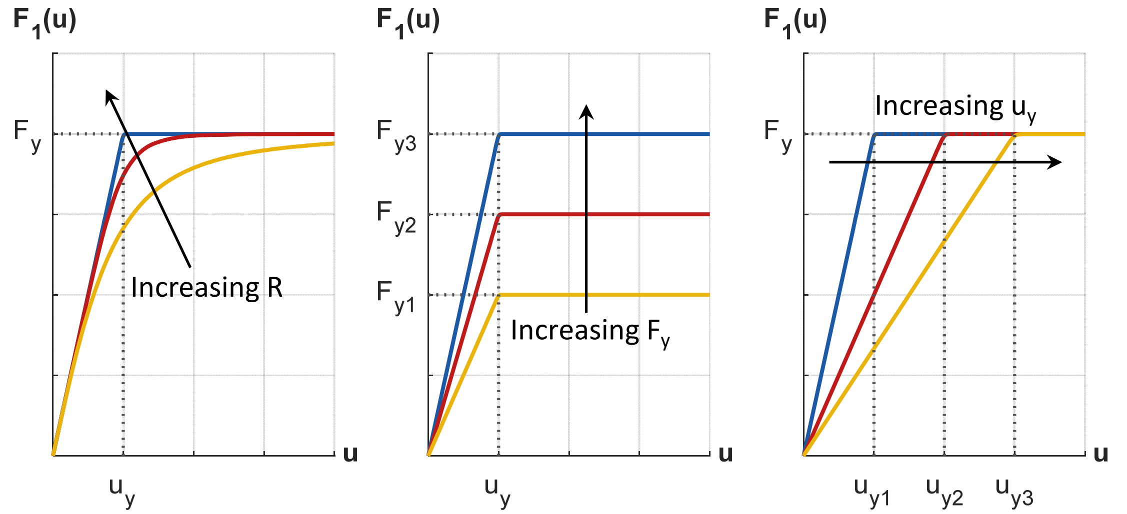

Figure 4. Effect of variation of different parameters on force $F_1(u)$ as a function of displacement when $b = 0$.

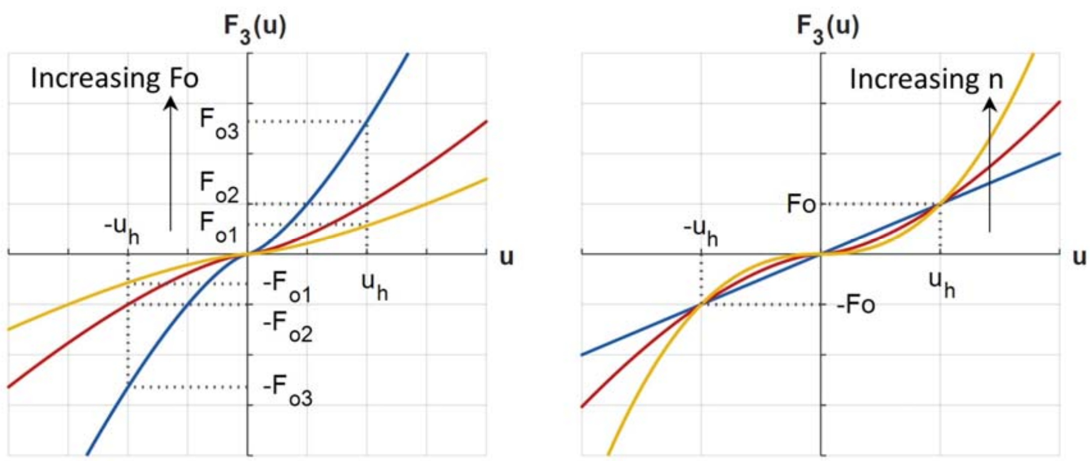

Figure 5. Effect of variation of different parameters on force $F_3(u)$ as a function of displacement.

It should be noted that the proposed model converges to the frequently-used kinematic-hardening bilinear model when the parameter R is set to a high value (e.g., $R \approx 40$) and F_o is set to zero. Under these conditions, the $F_3(u)$ term vanishes to zero and the high shear-strain hardening effect disappears.

Model parameters must be identified through optimization, minimizing the error between test-measured and model-predicted values. The optimization criterion can be selected from different features of the isolator force-displacement curve, e.g., force history, stiffness history, or dissipated energy, as extensively described and discussed in the following sections of this article. Initial values required to start the optimization process can be easily obtained as follows:

- For a given displacement cycle with shear strain γ, like the one shown in Figure 6(a), find by inspection the intersection between the curve and the force axis. This value can be used as an initial guess for parameter F_y.
- Measure the curve's slope k_{init} from the minimum (or maximum) displacement point, as displayed in Figure 6(a). Using this stiffness k_{init} and the initial estimation of F_y, calculate the initial estimation of u_y, through the expression $u_y = k_{init}/F_y$. It should be noted that strictly speaking, the stiffness k_{init} is actually including the high shear-strain hardening contribution to stiffness; however, this deviation could be neglected when obtaining initial values for the parameters.
- Visually estimate parameter b to match the secondary stiffness without considering high shear-strain hardening, as shown in Figure 6(a). In most cases, values for b range between 0.02 and 0.07.
- Given the initial estimations for F_y, u_y, and b, and using any value of R, plot a bilinear Menegotto-Pinto curve, using equation (2) for $F_1(u)$ and $F_2(u)$, as shown in the dashed blue curve in Figure 6(b.)
- Identify the hardening displacement u_h where the measured force noticeably departs from the force of the bilinear Menegotto-Pinto curve generated in the step above, as shown in Figure 6 (b). It should be noted that u_h is not a parameter to be identified but a fixed value.
- Select an initial value for F_o as the difference from the measured-force and the force-predicted by the Menegotto-Pinto model, both evaluated at u_h.
- Select an initial value for n to adjust the high shear-strain hardening ascending branch.
- Choose an initial value for R to match the transition between the initial and the secondary stiffness.

Once the parameters' initial values have been estimated independently for the different deformation cycles, a non-linear optimization procedure should be implemented to find optimal values, considering the displacement-dependent or the displacement-independent approach extensively described in the next sections of this article.

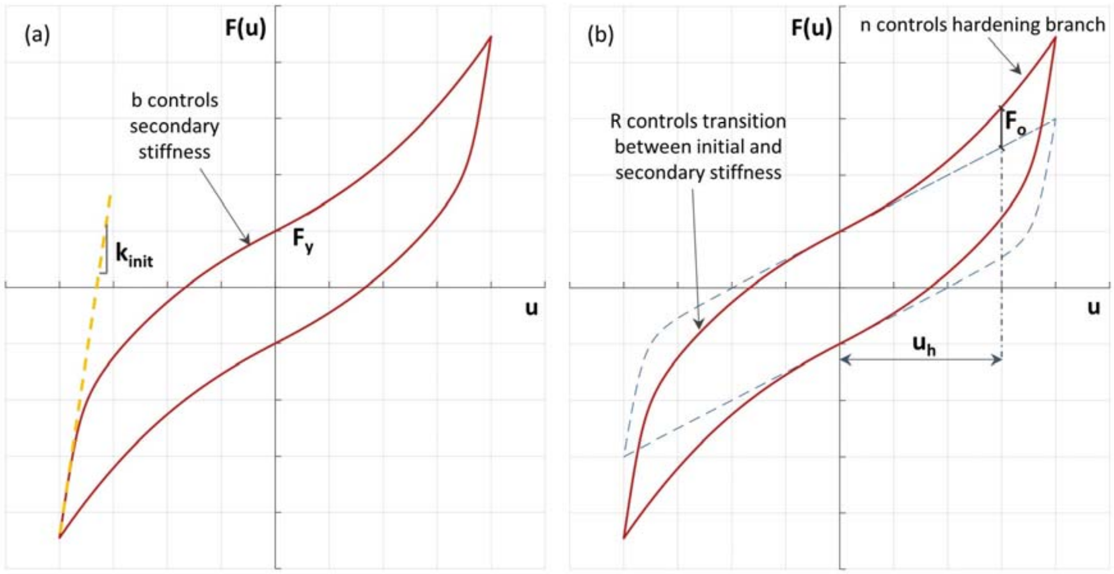

Figure 6. Parameters' initial-values estimation, using a cyclic deformation test.

As this model is intended for seismic isolator modeling under earthquake loads which involves reverse cyclic loading with varying amplitudes, a set of rules for unloading and reloading for inner cycles needs to be defined. In the original Menegotto-Pinto formulation, when the oscillator reverses its velocity at any displacement level smaller than the maximum displacement already reached during the response, the reloading curve could produce forces higher than the ones associated with the previous loading curve, violating the constraint imposed by the primary skeleton curve. In order to overcome this flaw in the original model, the storage of a previously undefined number of internal loops generated by the subsequential velocity reversals was required. These internal loops could be sequentially forgotten as the oscillator displacement exceeds the displacement where the loop was originated.

Ciampi et al. (1982) proposed a simplified procedure to correct this problem in the original Menegotto-Pinto model. This procedure only memorizes four curves, namely: i) the skeleton curve; ii) the ascending curve, starting at the reversal point with the minimum displacement value; iii) the descending curve, starting at the reversal point with the maximum displacement value; and iv) the current curve starting at the last reversal point. Despite its simplicity, this methodology has proven to give reasonably accurate results for modelling reinforcing steel bars subjected to reverse cyclic loading and is then implemented in this simplified model for elastomeric isolation bearings.

Figure 7 shows the original Menegotto-Pinto model erroneously following the blue line after a velocity reversal point, in this case, a small unloading followed by reloading. The model proposed in this work returns to the ascending curve defined by the reversal point with the minimum displacement. The transition curve after the last reversal point was analytically defined with the methodology proposed by Bosco et al. (2016).

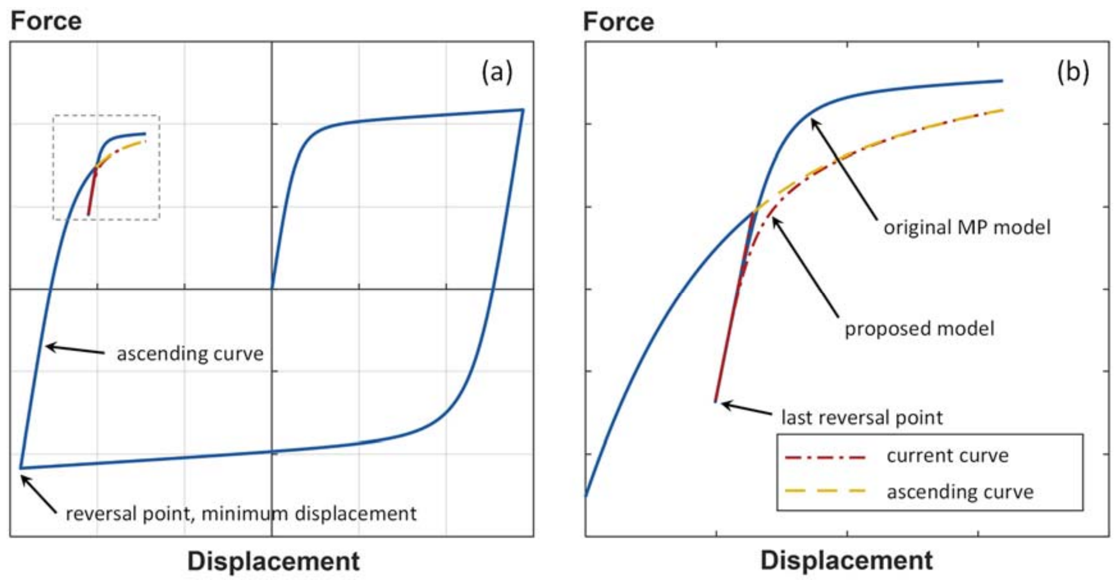

Figure 7. Proposed rules for seismic unloading and reloading: (a) force as a function of displacement, general view, and (b) reversal point, detailed view.

MODEL VALIDATION

Two types of verification were implemented to assess the simplified model's ability to represent the seismic isolator behavior under different load conditions. Firstly, the model was calibrated to fit four cyclic tests of different elastomeric isolators, including HDRBs and LRBs. Secondly, the proposed model was calibrated to fit two earthquake simulator tests of an HDRB isolator and an LRB isolator. The annular specimens used to calibrate the model are described in Tables 2 and 3 for cyclic tests and earthquake simulator tests, respectively. In these tables, ϕ is the external diameter of the isolator, ϕ_i is the internal diameter of the isolator, ϕ_{lead} is the lead-core diameter, and h_r is the total rubber height.

Table 2. Seismic isolator specimens calibrated through cyclic tests.

Specimen	Type	Geometry	Shear Strains
1	HDRB, Natural rubber compound.	$\phi = 750\ mm$ $\phi_i = 100\ mm$ $h_r = 128\ mm$	$\gamma = 0.50, 1.00, 1.50, 2.00$
2	LRB, Unfilled natural rubber compound	$\phi = 180\ mm$ $\phi_{lead} = 25\ mm$ $h_r = 36\ mm$	$\gamma = 0.85, 1.28, 1.70, 2.60$
3	LRB, Filled Natural rubber compound	$\phi = 750\ mm$ $\phi_{lead} = 150\ mm$ $h_r = 204\ mm$	$\gamma = 0.25, 0.50, 1.0, 1.25$
4	HDRB, Natural rubber compound.	$\phi = 600\ mm$ $\phi_i = 100\ mm$ $h_r = 133\ mm$	$\gamma = 0.25, 0.50, 1.0, 1.50$

Table 3. Seismic isolator specimens calibrated through earthquake simulator tests.

Specimen	Type	Geometry	Calibration Ground Motion
5	HDRB, Natural rubber compound	$\phi = 650\ mm$ $\phi_i = 100\ mm$ $h_r = 204\ mm$	ICA – 2007 Pisco (Peru) PGA = 0.50 g
6	LRB, Unfilled natural rubber compound	$\phi = 180\ mm$ $\phi_{lead} = 25\ mm$ $h_r = 36\ mm$	El Centro – 1940 Imperial Valley PGV = 50 cm/s

CYCLIC TEST CALIBRATION

The parameter calibration was performed using a least-squares approach to minimize the difference between test-measured and model-predicted values, based on initial values estimated using the procedure described in the section above. Different objective functions were used to define different sets of optimal model parameters. Frequently, a minimization of the deviation between the dissipated energy during a deformation cycle and its corresponding model-predicted value is selected as the optimality criterion (e.g., Ibarra et al. 2005). Another approach commonly used when calibrating model parameters considers minimizing the difference between the test-measured and the model-predicted forces during a given deformation cycle. However, as an oscillator's dynamic response depends on its tangent stiffness in the integration step under consideration, an objective function that minimizes the deviation in tangent stiffness is especially desirable.

To study how the objective function used during the optimization (minimization in this case) influences the model parameters, the cyclic test calibration was performed using five different objective functions, detailed in Table 4. For the objective functions minimizing the deviation of forces or stiffnesses throughout the loading history, two different approaches were implemented by computing an absolute difference and a relative difference between the experimental and the model-predicted values.

In the absolute difference case, the sum of the differences (in absolute value) between the measured and the model-predicted values during a deformation cycle is minimized, then the optimization process will tend to generate a better fit in the displacement range where the forces or the stiffnesses are high, as their contribution to the sum for the complete deformation cycle will be more relevant. On the other hand, in the relative difference case, the differences (also in absolute value) between the measured and the model-predicted values are normalized by the average between them. The normalized differences are afterward added for the complete deformation cycle. The optimal parameters obtained through the latter procedure should assure a more consistent agreement between the measured and the model-predicted values for the complete force-displacement curve.

The lateral stiffness was calculated through two different methods: (i) an "instantaneous" tangent stiffness, calculated as the force-displacement curve slope between two consecutive sampled values; and (ii) a secant stiffness, calculated as the slope of the force-displacement curve given a fixed displacement increment of 0.25 cm. In most cases, both approaches result in similar optimal parameters, but the extremely high stiffnesses observed for large shear displacements could generate numerical issues when using the "instantaneous" tangent stiffness approach, then the use of the secant stiffness was implemented.

For each different objective function, optimization was done in MATLAB's optimization toolbox using the *fmincon* function with the "interior-point" algorithm (MATLAB, 2020a). This function uses a Quasi-Newton method, which is based on Newton's method to minimize the objective function, but unlike the Newton method, the Hessian matrix does not need to be computed.

The complete set of objective functions was used to calibrate the cyclic test results for Specimen 1, vulcanized from natural rubber and annular-shaped with an external diameter ϕ of 750 mm, an internal diameter ϕ_i of 100 mm, sixteen 8-mm thick rubber layers, and fifteen 3-mm thick steel shims. The cyclic test was performed in the "Laboratory for dynamic testing and vibration control" at Pontificia Universidad Catolica de Chile on July 30th, 2014, under an expected axial load of 447 tonf. This specimen was subjected to a maximum shear strain of $\gamma = 2.0$, and the measured effective properties were $k_{eff} = 1.62\ tonf/cm$ (effective stiffness) and $\beta_{eff} = 12.4\%$ (effective damping). For further details on the testing setup, the reader is referred to De la Llera et al. (2004)

The influence of the selected objective function in the robustness of the different optimal parameter sets was assessed through the following steps:

- Different optimal parameter sets (*a*, *b*, *c*, *d*, and *e*) were calculated using each objective function described in Table 4.
- For each optimal parameter set, five different calibration errors were calculated using the five error indexes in Table 4.
- The five errors calculated with a specific error index were normalized by the minimum error associated with that index, i.e., the error of the optimal parameter set determined by the minimization of that specific error index.
- The last step was repeated for all the different error indexes defined in Table 4.

Table 4. Objective functions used to perform parameter calibration

Method	Objective function	Optimal parameter set	Error index used to fit model
1	$\min \quad ({E_d}^t - {E_d}^f)$	*a*	Dissipated energy during a complete deformation cycle, deviation between test-measured and model-fitted values.
2	$\min \sum_i ({F_i}^t - {F_i}^f)^2$	*b*	Force for each sampled displacement, squared absolute deviation between test-measured and model-fitted values.
3	$\min \sum_i \left(\frac{({F_i}^t - {F_i}^f)}{\lvert {F_i}^t \rvert + \lvert {F_i}^f \rvert} \right)^2$	*c*	Force for each sampled displacement, squared relative deviation between test-measured and model-fitted values.
4	$\min \sum_i ({K_i}^t - {K_i}^f)^2$	*d*	Secant stiffness for each sampled displacement, squared absolute deviation between test-measured and model-fitted values.

5	$\min \sum_{i} \left(\frac{(K_i{}^t - K_i{}^f)}{\lvert K_i{}^t \rvert + \lvert K_i{}^f \rvert} \right)^2$	e	Secant stiffness for each sampled displacement, squared relative deviation between test-measured and model-fitted values.

where:

$E_d{}^t = 1/2 \sum_{i=1}^{m-1} (F_{i+1}{}^t + F_i{}^t)(u_{i+1} - u_i)$, total test-measured dissipated energy for a given displacement cycle.

$E_d{}^f = 1/2 \sum_{i=1}^{m-1} (F_{i+1}{}^f + F_i{}^f)(u_{i+1} - u_i)$, total model-fitted dissipated energy for a given displacement cycle.

u_i = sampled displacement i, during a cyclic test.

m = total number of sampled displacements during a cyclic test.

$F_i{}^t$ = test-measured force at step i, during a cyclic test.

$F_i{}^f$ = model-fitted force at step i, during a cyclic test.

$K_i{}^t$ = test-measured secant stiffness at step i, during a cyclic test.

$K_i{}^f$ = model-fitted secant stiffness at step i, during a cyclic test.

For each optimal set of parameters, those that minimize the five different objective functions, the other four objective functions' relative errors are shown in Figure 8. The optimal set of parameters *b*, determined through minimization of absolute force deviation, shows the smallest variability between relative errors, meaning that the deviation between the test and the model-predicted values is closest, regardless of the error index used to measure this deviation. On the other extreme, for the optimal parameter set *e*, determined by minimization of the relative secant stiffness deviation, the level of agreement between the test and the model-predicted values depends strongly on which measure of error was implemented. Consequently, for Specimen 1 modeling, optimal parameter set *b* is better than optimal parameter set *e,* as it produces errors using all five measures of deviation that are closer to the minimum values.

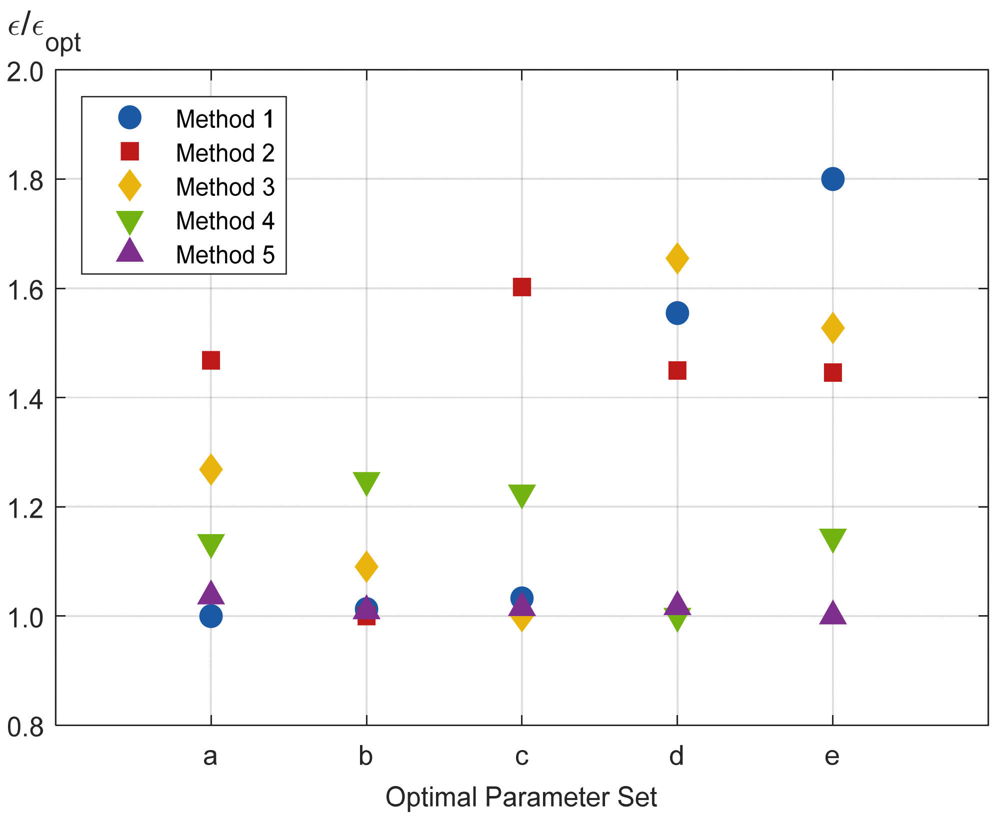

Figure 8. A comparison of errors calculated using the five objective functions in Table 4 for a given optimal parameter set, normalized to the minimum error for each optimization criterion.

Figure 9 shows schematically for Specimen 1, at a given shear strain of $\gamma = 2.0$, how the objective function's selection influences the optimal parameter set and their associated model-predicted values. When dissipated energy is selected as the calibration criterion, the optimization process tends to equalize the areas enclosed by the force-displacement curves, and then some significant differences in lateral stiffness can be observed mainly in the low to moderate displacement cycles. Since the solution of the differential equation of motion depends on adequately capturing changes in the lateral tangent stiffness at each integration step, this approach could lead to significant errors in the oscillator seismic response calculation.

Based on the previous comment, an objective function based on minimizing the difference in stiffness between the measured and the model-predicted values, would appear to be the most logical choice. However, the specimen under consideration is strongly characterized by its noticeable hardening in the high displacement range, then a substantial stiffness increase is expected at large displacements. For specimens that exhibit strong hardening, the stiffness can become very large, and therefore the use of this objective function, even though the general agreement between the experimental and the model-predicted values is acceptable, will minimize deviations between measured and computed stiffness in this region but may produce larger errors in portions of the hysteretic cycle in which the stiffness is small, which are of interest as those would be producing larger displacement increments.

As can be seen in the central plot (b) in Figure 9, when a force deviation minimization criterion is used to define the optimal parameters, the model fits with reasonable accuracy the experimental test data in the complete displacement range under analysis, then the stiffnesses and the non-linear forces predicted by the model are quite similar to the ones in the experimental test. Based on this fact, an absolute force-based error index (Method *b* in Table 4) was selected as the optimization criterion for the rest of this study.

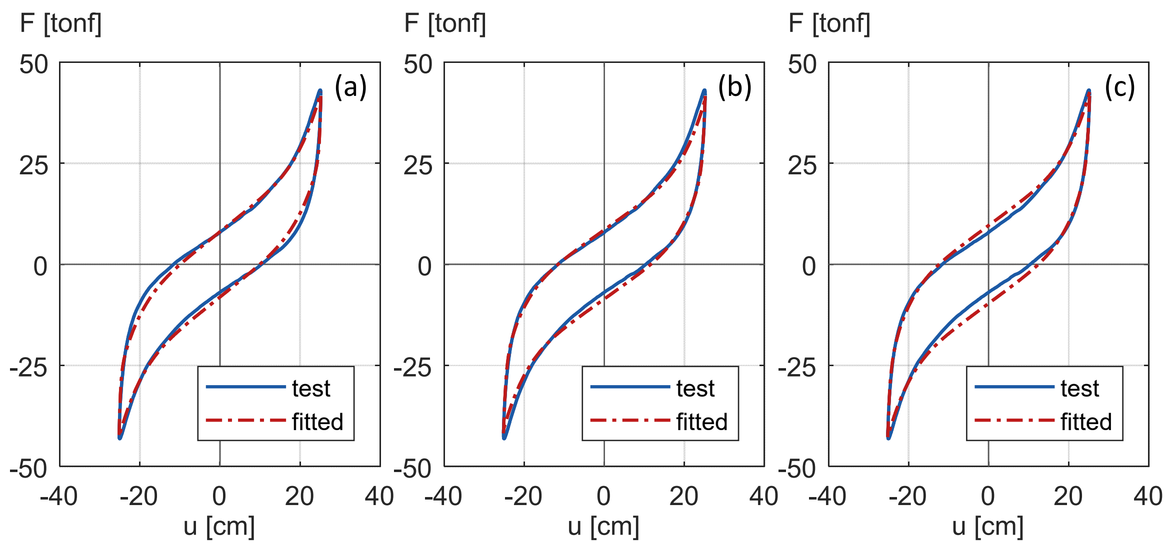

Figure 9. Comparison of the experimental test data (Specimen 1, $\gamma = 2.0$) and the model-fitted data using different objective functions to identify the optimal set of parameters: (a) dissipated energy deviation minimization; (b) force deviation minimization; and (c) stiffness deviation minimization.

As it has been widely established in the literature (Kikuchi and Aiken 1997), the constitutive models that do not use differential equations on their formulation generally need to update their parameters as a function of the specimen shear strain (hereafter referred to as displacement-dependent parameters). A sequential approach was implemented to study how the quality of the fit is affected by this displacement dependency. In the first stage of the optimization process, the model parameters were calibrated independently for each shear strain in the cyclic test, getting the best possible fit and implying that all parameters were displacement-dependent. This allows the identification of the parameters that are more sensitive to the level of deformation. Afterward, in the second stage of the optimization procedure, the displacement-dependent parameters were gradually constrained to check their displacement-independency. The sequence of the parameters to be constrained was selected by minimizing the growth of the fitting error.

Figure 10 shows the experimental and the model-predicted force-displacement curves for the first stage of the calibration procedure when most parameters are assumed displacement-dependent, i.e., their values change as a function of the shear strain. An excellent agreement between the experimental and the model-predicted data is observed for all specimens under analysis. Optimal parameters are listed in Table 5.

Table 5. Model-calibrated parameters for all specimens, when the best possible fit is obtained by setting many displacement-dependent parameters. (Displacement-dependent parameters are shown in bold characters).

Specimen	γ	u (cm)	F_y (tonf)	u_y (cm)	b	R	F_o (tonf)	n
1	0.50	6.40	**7.79**	**0.17**	**0.04**	**0.65**	**3.31**	4.85
	1.00	12.80	**8.78**	**0.19**	**0.02**	**0.69**	**3.31**	4.85
	1.50	19.20	**7.90**	**0.22**	**0.02**	**0.93**	**1.42**	4.85
	2.00	25.60	**9.12**	**0.37**	**0.03**	**1.94**	**0.55**	4.85
2	0.85	3.06	**0.51**	**0.15**	**0.07**	**3.61**	0.36	1.00
	1.28	4.61	**0.50**	**0.10**	**0.04**	**1.84**	0.36	1.00
	1.70	6.12	**0.56**	**0.05**	**0.01**	**0.66**	0.36	1.00
	2.60	9.36	**0.51**	**0.09**	**0.02**	**0.95**	0.36	1.00
3	0.25	5.10	**80.36**	**0.83**	**0.002**	**0.56**	1.55	3.50
	0.50	10.20	**64.94**	**0.50**	**0.002**	**0.53**	1.55	3.50
	1.00	20.40	**28.98**	**0.37**	**0.009**	**0.82**	1.55	3.50
	1.25	25.50	**21.58**	**0.26**	**0.007**	**0.70**	1.55	3.50
4	0.25	3.33	**6.88**	**0.27**	**0.038**	**0.39**	0.34	6.00
	0.50	6.65	**5.77**	**0.16**	**0.023**	**0.39**	0.34	6.00
	1.00	13.30	**3.32**	**0.31**	**0.072**	**1.56**	0.34	6.00
	1.50	19.95	**4.03**	**0.39**	**0.068**	**1.95**	0.34	6.00

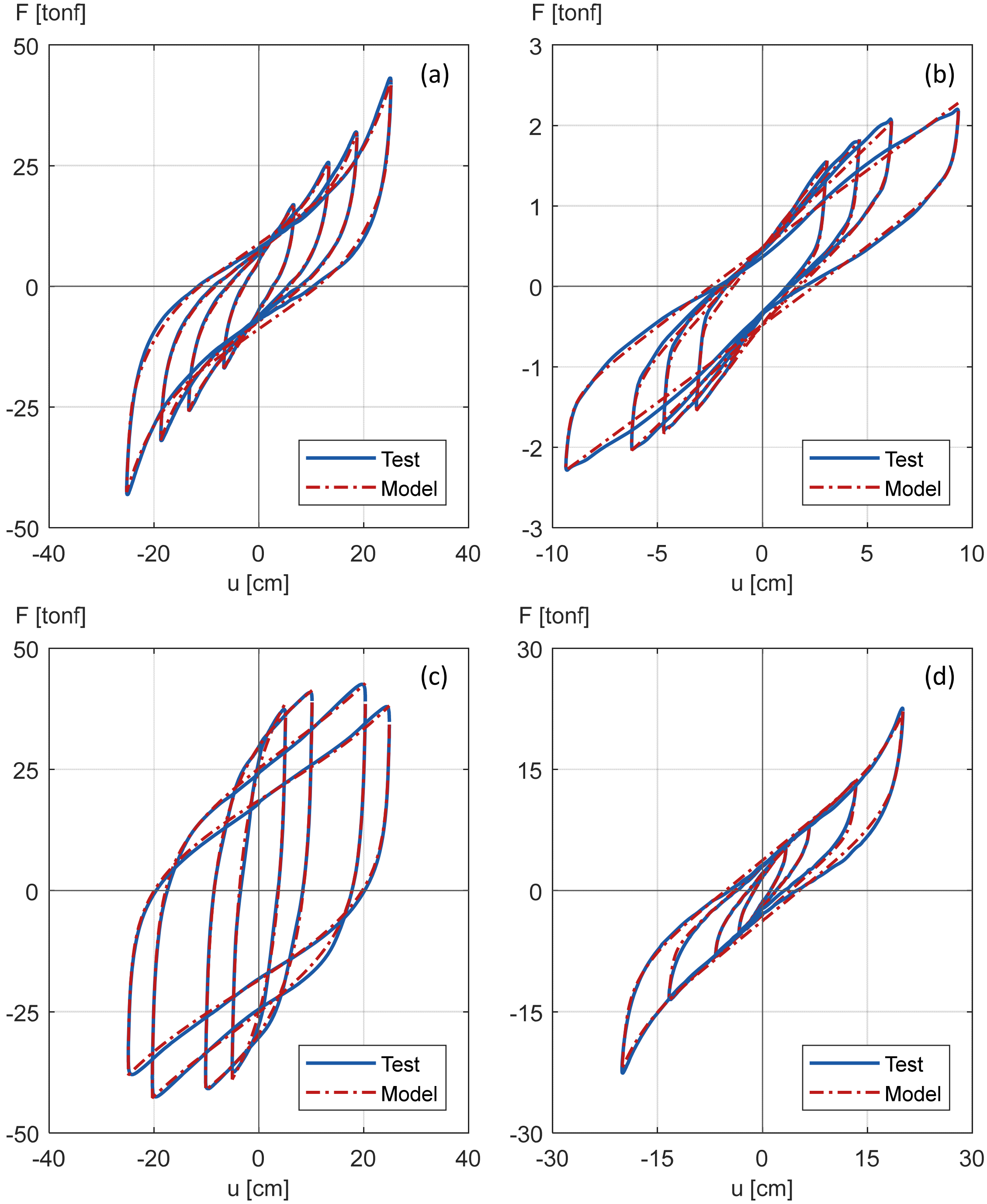

Figure 10. Experimental test data and best model-fitted data for specimens: (a) 1, (b) 2, (c) 3, and (d) 4, as described in Table 2. The model parameters used in each Specimen are listed in Table 5.

Figure 11 shows the calibration relative error in Specimen 1 as a function of the number of displacement-dependent parameters. This sensitivity analysis was performed for the five objective functions defined in Table 4. The best fit was considered to be the one obtained when five out of six parameters were set to be displacement-dependent. This case did not show any noticeable decrease in the fit quality compared with the case where all parameters were considered displacement-dependent. These parameters were sequentially constrained to be displacement-independent (i.e., assuming constant values) to assess how the fit's quality decreases as the number of displacement-dependent parameters decreases.

For Specimen 1, it can be seen that when setting only two displacement-dependent parameters (b and F_o), the quality of the fit is quite similar to the case with five displacement-dependent parameters, regardless of the objective function used for the optimization, excepting the case where the dissipated-energy objective function was used (Method 1).

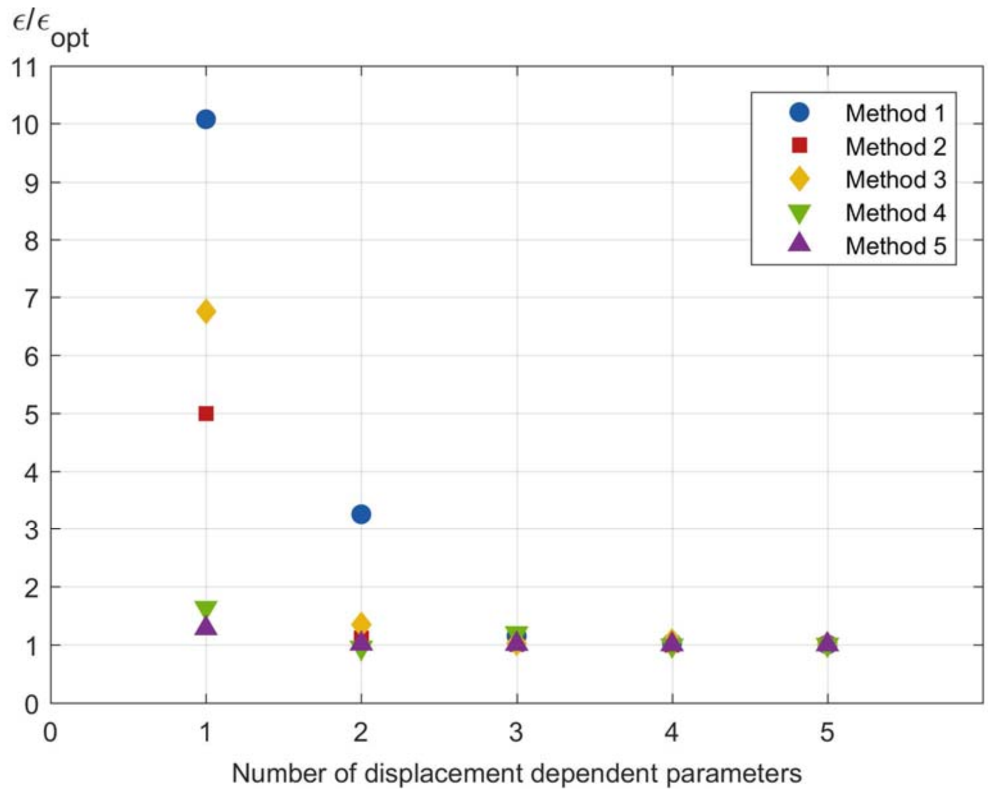

Figure 11. Model-fitted relative error as a function of the number of displacement-dependent parameters, Specimen 1.

A similar trend between the quality of the fit and the number of displacement-dependent parameters was observed for the other specimens used in this study. Therefore, with the proposed model, generally speaking, there is no need to consider a large number of displacement-dependent parameters to get an accurate analytical prediction. Figure 12 shows the comparison between the experimental and the model-predicted force-displacement curves when only two displacement-dependent parameters are considered for Specimens 1, 2, and 3, and when only one displacement-dependent parameter is considered for Specimen 4. These updated parameter sets are listed in Table 6.

Even though the updated parameters in Table 6 are considerably simpler, as the number of displacement-dependent parameters was reduced relative to those listed in Table 5, the agreement between the test results and the model-predicted values is still entirely satisfactory.

Table 6. Model-calibrated updated parameters for all specimens. Displacement-dependent parameters are shown in bold characters.

Specimen	γ	u (cm)	F_y (tonf)	u_y (cm)	b	R	F_o (tonf)	n
1	0.50	6.40	8.40	0.30	**0.05**	1.05	**3.31**	4.85
	1.00	12.80	8.40	0.30	**0.04**	1.05	**3.31**	4.85
	1.50	19.20	8.40	0.30	**0.03**	1.05	**1.42**	4.85
	2.00	25.60	8.40	0.30	**0.03**	1.05	**0.55**	4.85
2	0.85	3.06	0.54	0.06	**0.02**	**1.00**	0.36	1.00
	1.28	4.61	0.54	0.06	**0.02**	**0.99**	0.36	1.00
	1.70	6.12	0.54	0.06	**0.02**	**0.77**	0.36	1.00
	2.60	9.36	0.54	0.06	**0.01**	**0.75**	0.36	1.00
3	0.25	5.10	**55.87**	0.49	**0.009**	0.61	1.55	3.50
	0.50	10.20	**53.27**	0.49	**0.004**	0.61	1.55	3.50
	1.00	20.40	**39.86**	0.49	**0.005**	0.61	1.55	3.50
	1.25	25.50	**27.96**	0.49	**0.007**	0.61	1.55	3.50
4	0.25	3.33	4.13	0.43	0.076	**0.75**	0.34	6.00
	0.50	6.65	4.13	0.43	0.076	**0.73**	0.34	6.00
	1.00	13.30	4.13	0.43	0.076	**0.81**	0.34	6.00
	1.50	19.95	4.13	0.43	0.076	**2.31**	0.34	6.00

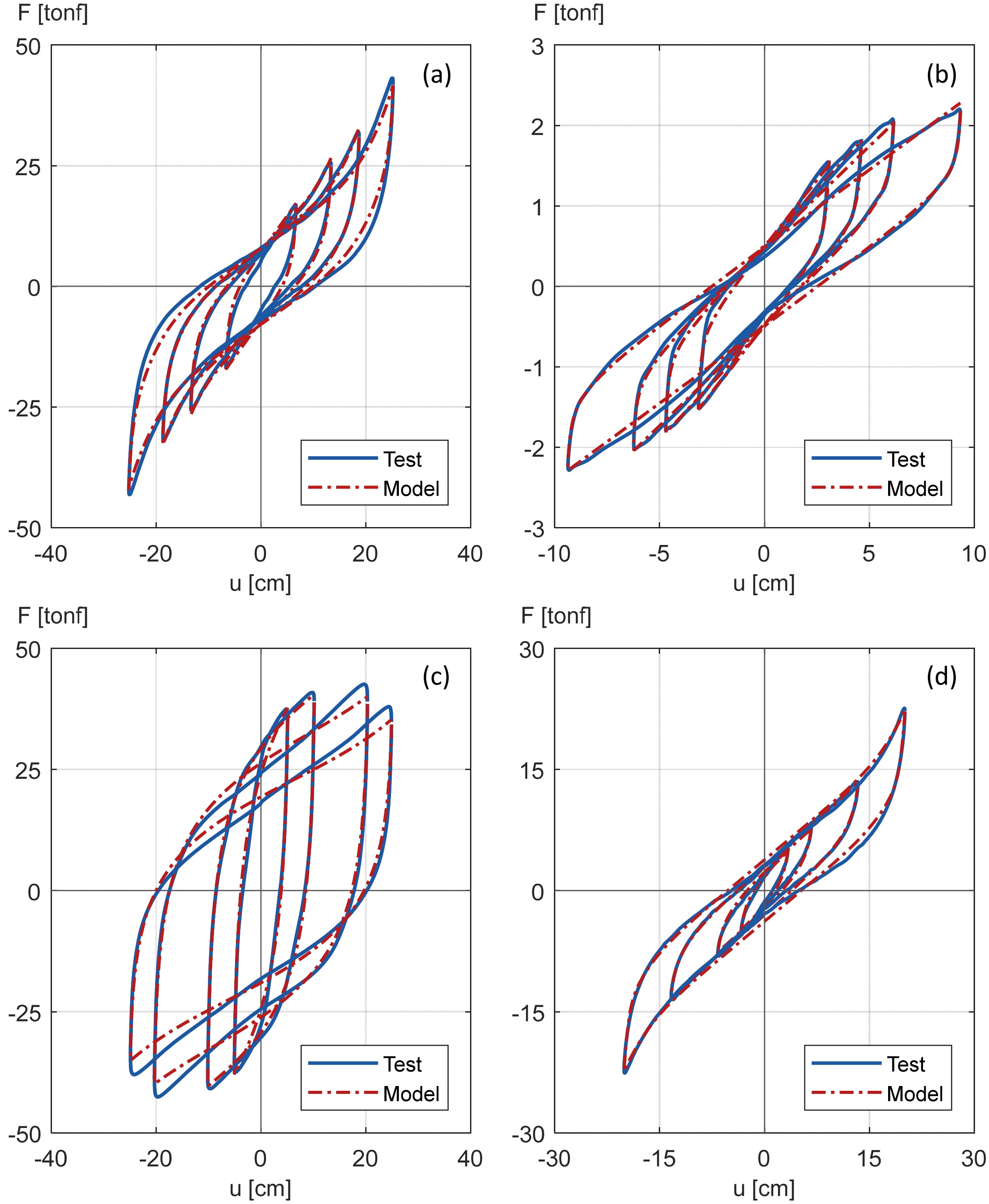

Figure 12. Experimental test and simplified model-fitted data for: (a) Specimen 1 with b and F_o displacement-dependent; (b) Specimen 2 with b and R displacement-dependent; (c) Specimen 3 with F_y and b displacement-dependent; and (d) Specimen 4 with R displacement-dependent. The model parameters for each case are listed in Table 6.

A quantitative comparison between the performances of the proposed model and the Kikuchi and Aiken model is presented, based on the cyclic test results of Specimen 1. Models are compared using the coefficient of determination R^2 of three different metrics of the force-displacement curve, namely: (i) the dissipated energy, (ii) the force history, and (iii) the stiffness history, all of them measured for all the displacement cycles. Coefficients of determination R^2 were calculated using the equation:

$$R^2 = 1 - \frac{\sum_{i=1}^{n}(y_i - \hat{y}_i)^2}{\sum_{i=1}^{n}(y_i - \bar{y})^2} \tag{3}$$

where y_i is the test-measured metric at displacement step i, $\hat{y}_i$ is the model-predicted metric at displacement step i, and $\bar{y} = \sum_{i=1}^{m} y_i/m$ is the mean of the test-measured metric, where m is the total number of sampled displacements during a cyclic test. For the proposed model, the R^2 results for the best-fit scenario (five displacement-dependent parameters) and the simpler but accurate scenario (two displacement-dependent parameters) are reported.

Table 7. Coefficient of determination R^2 for the proposed model and the Kikuchi and Aiken Model.

Predicted metric	Proposed model Simpler scenario (two displacement dependent parameters)	Proposed model Best-fit scenario (five displacement dependent parameters)	Kikuchi and Aiken Model $u = -0.084\,\gamma + 0.340$ $h_{eq} = -0.037\,\gamma + 0.194$ $n = 1.569\,\gamma + 0.017$ a from Eq., but if $\gamma > 1.0$ $a = 36$ b from Eq., but if $\gamma > 1.5$ $b = 16$ $c = 6.0$
Dissipated energy	0.957	0.997	0.995
Force history	0.931	0.933	0.937
Stiffness history	0.572	0.594	0.537

As shown in Table 7, the R^2 coefficients of the proposed model and the Kikuchi and Aiken model are very similar when most parameters are displacement-dependent, with slightly larger (better) R^2 coefficients for the proposed model when predicting either dissipated energy or stiffness history. The proposed-model simpler set of parameters, in which we only used two displacement-dependent parameters, delivers R^2 coefficients that are just slightly lower than the Kikuchi and Aiken ones for dissipated energy and force history but actually larger (better) for stiffness history, still predicting all metrics with enough accuracy.

The presented simplified model constitutes a suitable alternative for isolation bearings modeling, given the quality of its predictions. Additionally, it is relevant to highlight that all its parameters are related to force-displacement curves' observable characteristics, constituting a noticeable advantage when compared to other available models. For example, the Kikuchi and Aiken model uses parameters (*a* and *b*) proposed to be computed with equations related to other parameters directly determined from the force-displacement curve. Still, the authors noted that those equations only apply to a particular range of displacements, and the parameters directly determined from the curve need to be constrained for the equations to work properly. To overcome these flaws, the authors proposed using the equation in a given displacement range and using an arbitrary constant for other cases, making the calibration procedure noticeably more difficult.

EARTHQUAKE TEST CALIBRATION

The capability of the proposed simplified model to adequately represent the force-displacement relationship of different types of seismic isolators under earthquake loads was assessed by comparing its analytically predicted values with the results of two different earthquake simulator tests. In this case, the model parameters were identified as follows:

- As the isolators' cyclic test results were available for both cases, an initial and displacement-independent estimation of the six model parameters was performed.
- An analysis of the sequence that best improves the fit quality by incrementally redefining some parameters as displacement-dependent was carried out.
- Given parameter p_i to be updated as displacement-dependent, its identification was performed through a force-error minimization procedure (i.e., Method 2 in Table 4) for the complete earthquake displacement history. In this case, the output of the optimization process is not a single value for the parameter p_i, but several (γ, p_i) ordered pairs. The selected γ values were arbitrarily defined based on the displacement history of the earthquake ground motion under analysis.
- The last step was repeated for the following parameter p_j selected to be updated as displacement-dependent.

It should be noted that in the case of an earthquake test calibration, a functional form relating the parameter being calibrated with the isolator shear strain needs to be selected, then several functional forms were studied. However, results suggest that the selected functional form does not have a significant effect on the ability of the model to predict the isolator behavior under a given displacement history. Consequently, only two functional forms to describe the variation of the parameters with changes in the level of strain, were selected based on their simplicity. These functional forms will be hereafter referred to as FF1 and FF2 and are displayed in Figure 13.

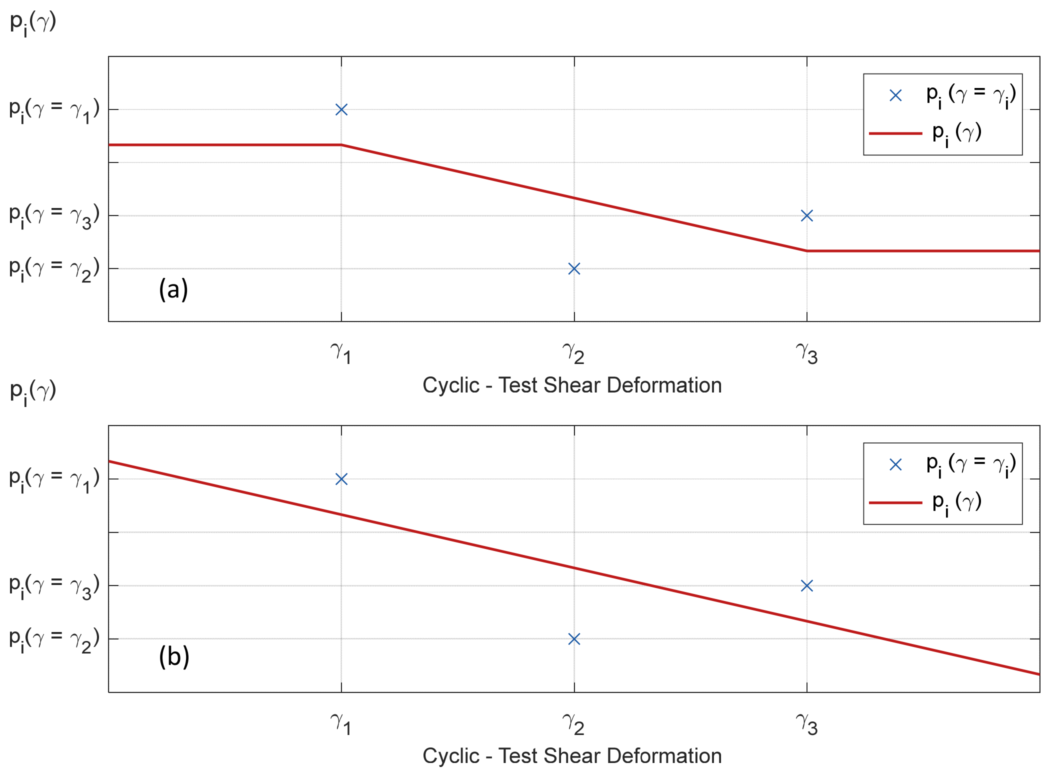

Figure 13. Displacement-dependent parameter p_i as a function of the isolator shear strain, when calibrating with earthquake test results: (a) Functional Form 1, FF1; and (b) Functional Form 2, FF2.

The following paragraphs describe the main characteristics and features of the earthquake simulation tests used to calibrate the simplified model.

Earthquake simulation test calibration - Case 1

The *Building Nonstructural Components and Systems (BNCS)* (Chen et al. 2013) project considered the construction and earthquake simulation testing of a one to one scale specimen of a five-story reinforced concrete building, equipped with several nonstructural components. The project considered tests on a fixed-base configuration and on an isolated-base configuration that took place between April 2012 and May 2012 at the George E. Brown, Jr., Network for Earthquake Engineering Simulation (NEES) unidirectional Large High-Performance Outdoor Shake Table at the University of California, San Diego (UCSD). In the base-isolated configuration, the building was subjected to seven ground motions records, representative of the seismicity in California, a central area of Alaska, and a subduction zone in South America. For the simplified model calibration, a record from the 2007 Mw 8.0 Pisco-Peru earthquake (ICA ground motion record) was selected. In the *BNCS* project, the original ICA ground motion record was scaled by a factor of 1.4; then, the test specimen was subjected to a maximum ground acceleration of 0.50 g, a peak input velocity of 62.59 cm/s, and a peak input displacement of 12.92 cm. This ground motion record was the most demanding one used in the isolated-base configuration of the building, so it was selected to test the ability of the simplified model to capture the hardening effect adequately. The building was supported on four high damping rubber isolators (HDRB), whose geometric and material characteristics are listed in Table 4, as Specimen 5.

The force-displacement curve in any of the isolators was required to perform the model calibration. As this information was not directly reported, the induced inertial forces in the building and the resultant shear force demand over the isolation level were estimated by using the accelerometer readings on each floor and their corresponding floor masses lumped at the center of mass of each floor. The isolators' relative displacements were calculated through double integration of the accelerometer readings below and above the isolators.

Figure 14 shows the experimentally measured and the model-predicted force-displacement curves for Specimen 5. The fitted curve on the left was computed using five displacement-dependent parameters (all but n), while the fitted curve on the right was computed with all six parameters as constants (i.e., displacement-independent parameters). The model parameters for both cases are detailed in Table 8. In the case where displacement-dependent parameters were considered, the functional form FF1 was used to relate the parameter with the isolator shear strain. It can be seen that while the fit obtained using five displacement-dependent parameters is better, the one computed with the much simpler displacement-independent (i.e., constant) parameters still provides a very good match of measured hysteretic behavior, being this latter approach good enough for practical engineering applications.

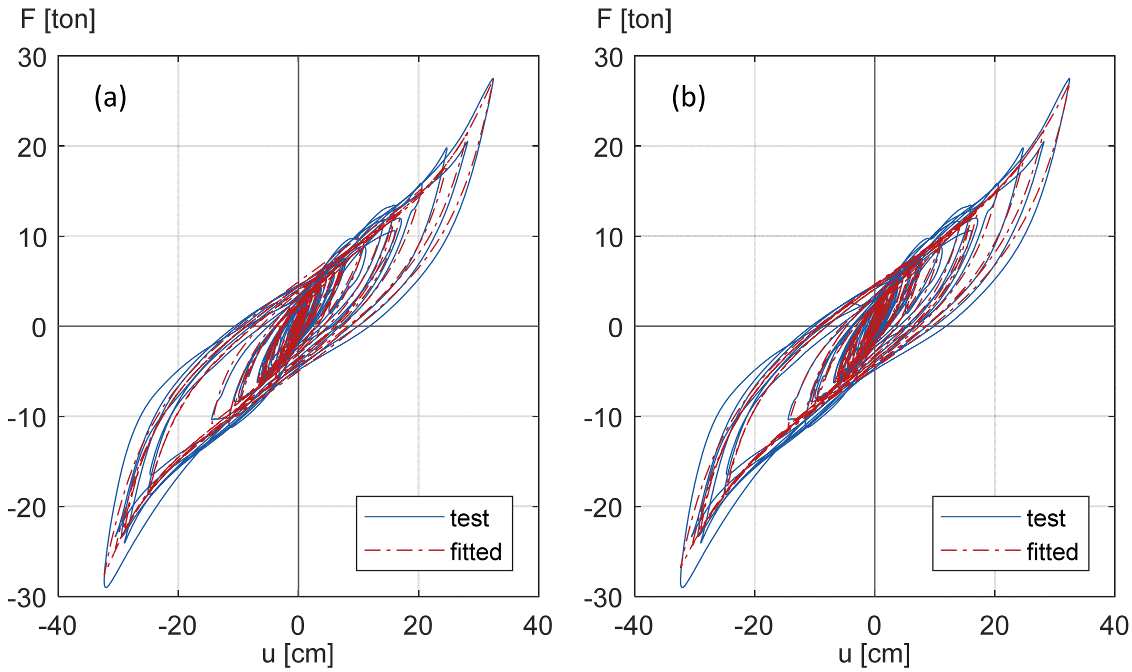

Figure 14. Force-displacement curves for the experimental test and the model-fitted data under the ICA ground motion record: (a) Five displacement-dependent parameters; and (b) No displacement-dependent parameters, as detailed in Table 8.

Table 8. Model-calibrated parameters for Specimen 5 under the ICA ground motion record. Displacement-dependent parameters are shown in bold characters.

Case	γ	u (cm)	F_y (tonf)	u_y (cm)	b	R	F_o (tonf)	n
(a)	0.5	10.2	**7.29**	**2.98**	**0.20**	**1.16**	**0.55**	4.65
	1.0	20.4	**6.63**	**2.90**	**0.18**	**1.30**	**1.08**	4.65
	1.5	30.6	**7.29**	**3.10**	**0.20**	**1.16**	**0.77**	4.65
(b)	any	any	6.83	2.93	0.19	1.24	1.21	3.97

Figure 15 shows the force-history response as a function of time for the experimental and the model-predicted data, using the model parameters detailed in Table 8.

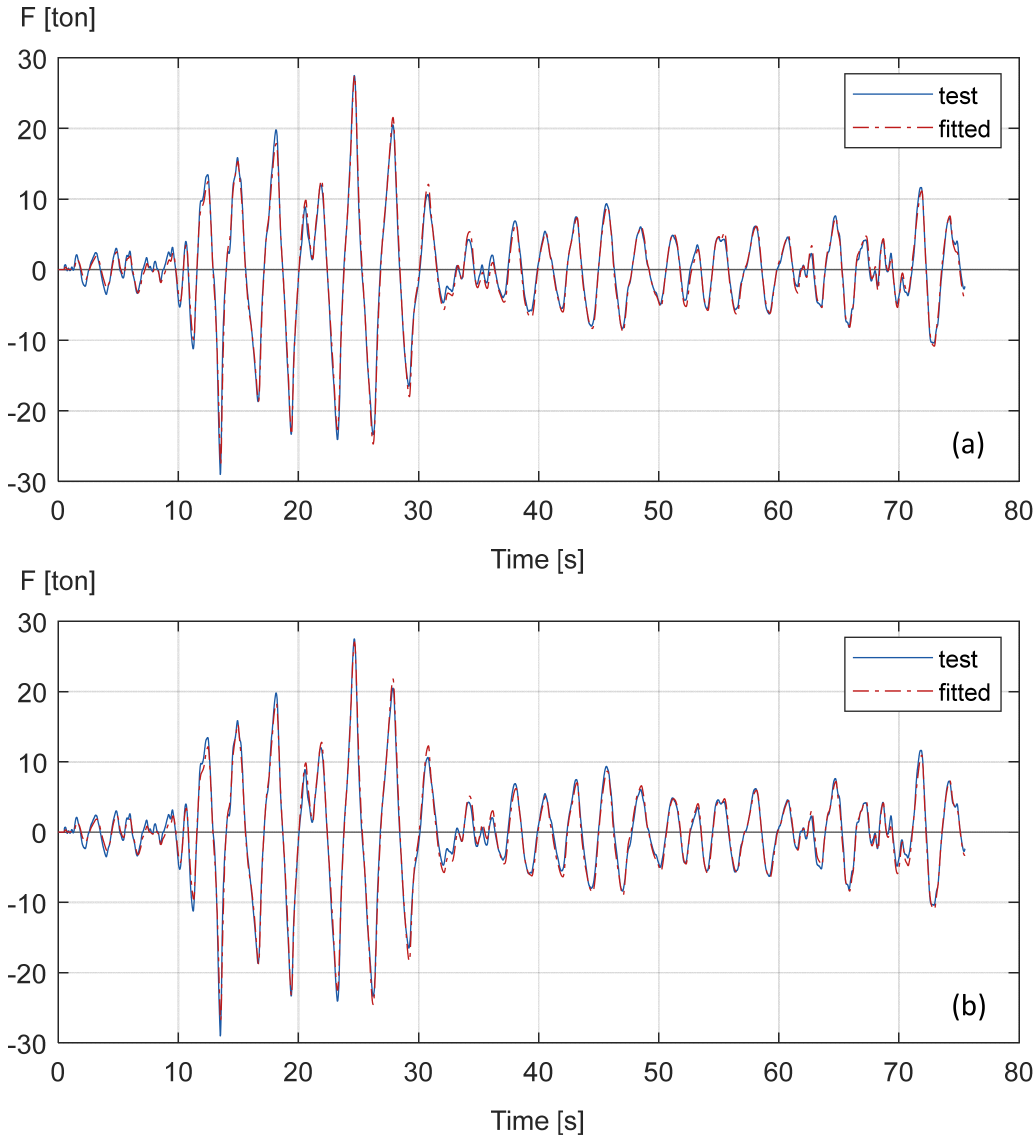

Figure 15. Force as a function of time for the experimental test and the model-fitted data, under the ICA ground motion record: (a) Five displacement-dependent parameters and; (b) No displacement-dependent parameters, as detailed in Table 8.

Earthquake simulation test calibration - Case 2

The second earthquake simulation test was taken from the seminal work of Kikuchi and Aiken (1997). The specimen under analysis is a Lead-Rubber Bearing (LRB) described as Specimen 6 in Table 3. For any further detail on the test features and specifications, the reader is referred to Kikuchi and Aiken (1997), where this specimen is identified as *lead-rubber bearing*. The earthquake simulation test was performed with the well-known NS component of *El Centro* ground motion record from the 1940 Imperial Valley earthquake.

Figure 16 shows the experimentally measured and the model-predicted force-displacement curves for Specimen 6. Again the fitted curve on the left was computed setting five out of the six parameters to be displacement-dependent (all but u_h), while the fitted curve on the right was computed setting all six parameters as constant (i.e., displacement-independent). The model parameters for both cases are detailed in Table 9. In the case where displacement-dependent parameters were considered, the functional form FF1 was used to relate the parameter with the shear strain. Similar to the results shown in Figure 14 and Figure 15, it can be seen that the model-predicted values using constant parameters provide good results that are enough for engineering design practice.

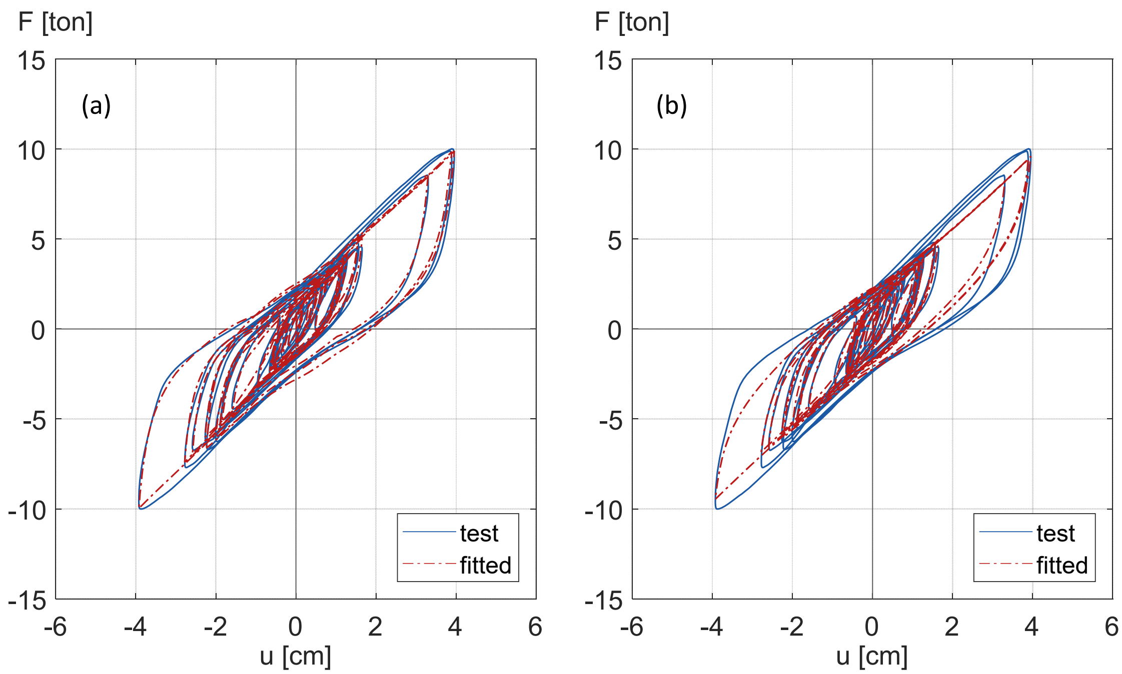

Figure 16. Force-displacement curves for the experimental test and the model-fitted data, under *El Centro* ground motion record: (a) Five parameters displacement-dependent; and (b) No displacement-dependent parameters, as detailed in Table 9.

Table 9. Model-calibrated parameters for Specimen 6, under the *El Centro* ground motion record. Displacement-dependent parameters are shown in bold characters.

Case	γ	u (cm)	F_y (tonf)	u_y (cm)	b	R	F_o (tonf)	n
(a)	0.16	1.5	**3.06**	**0.12**	**0.04**	**0.68**	2.93	**1.42**
	0.48	2.5	**3.37**	**0.13**	**0.03**	**1.27**	3.16	**1.52**
(b)	any	any	2.69	0.14	0.04	1.00	3.80	1.30

Figure 17 shows the force-history response as a function of time, for the experimental and the model-predicted data, using the model parameters detailed in Table 9.

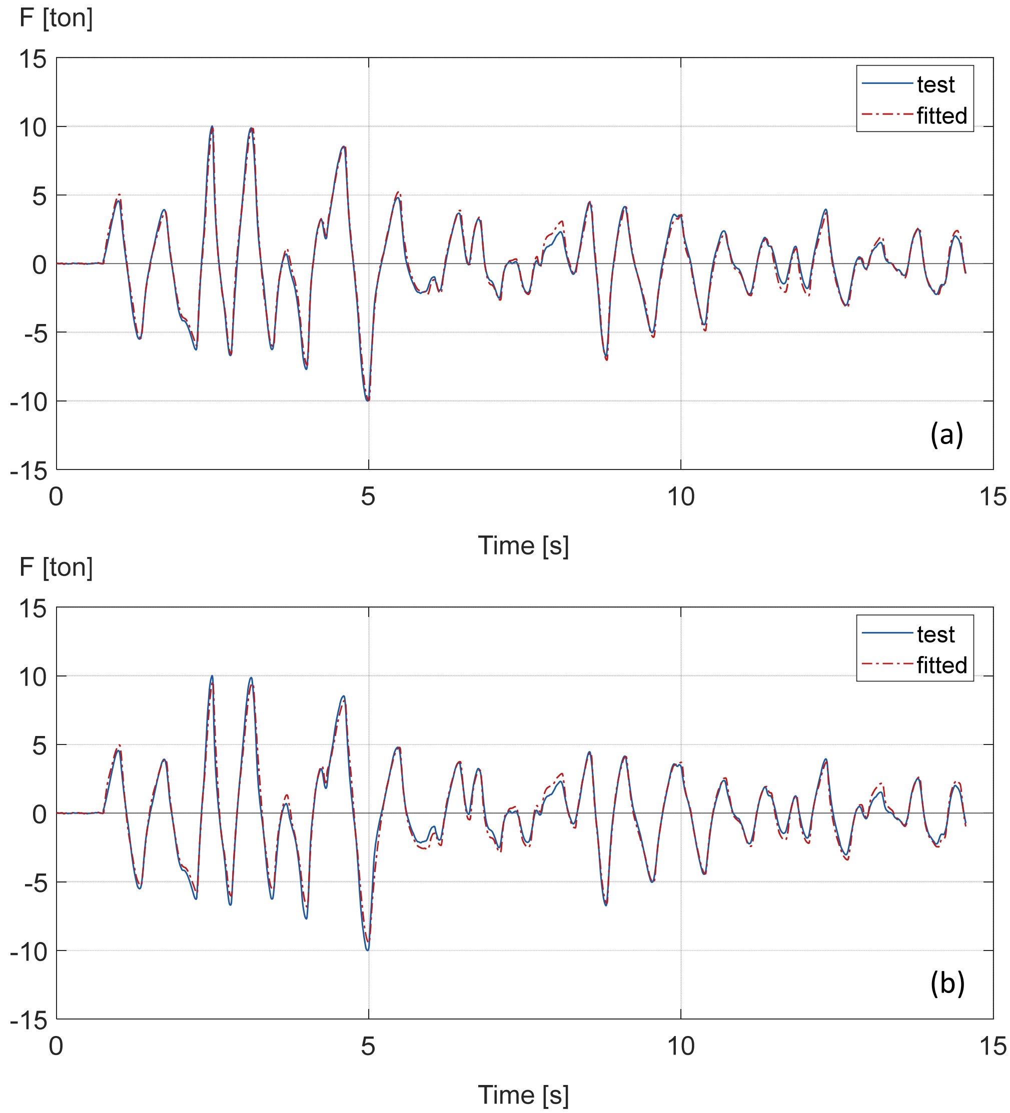

Figure 17. Force as a function of time for the experimental test and the model-fitted data, under the *El Centro* ground motion record: (a) Five displacement-dependent parameters; and (b) No displacement-dependent parameters, as detailed in Table 9.

In Figure 18, an analysis of the tradeoff between considering an increasing number of displacement-dependent parameters in exchange for minimizing the error is presented. As it should be expected, the error decreases as the number of displacement-dependent parameters increases; however, a distinct difference is observed for Specimen 5 (HDRB) relative to Specimen 6 (LRB), as the former is less sensitive to the number of displacement-dependent parameters. This condition can be confirmed by comparing the force-displacement curves in Figure 14, which look quite similar despite their difference in the definition of parameters. The total error of the model-fitted force-history increases only 20% when comparing the simplest model with no displacement-dependent parameters, with the most complex model, with five displacement-dependent parameters.

On the other hand, Specimen 6 is more sensitive to model parameters definition, with a fitting error that is 75% higher in the simplest case (no displacement-dependent parameters) relative to the most complex case (five displacement-dependent parameters). However, a noticeable improvement in the fit quality occurs when considering only one parameter as displacement-dependent (R in this case). In this new scenario, the relative error reduces from 75% to being only 15% higher than the best fit case. As shown in Figure 18, as more parameters become displacement-dependent, the additional fitting improvement is rather small. As previously stated in this article, the choice of the functional form used to evaluate the displacement-dependent parameters does not significantly influence the quality of the fit for both cases under study.

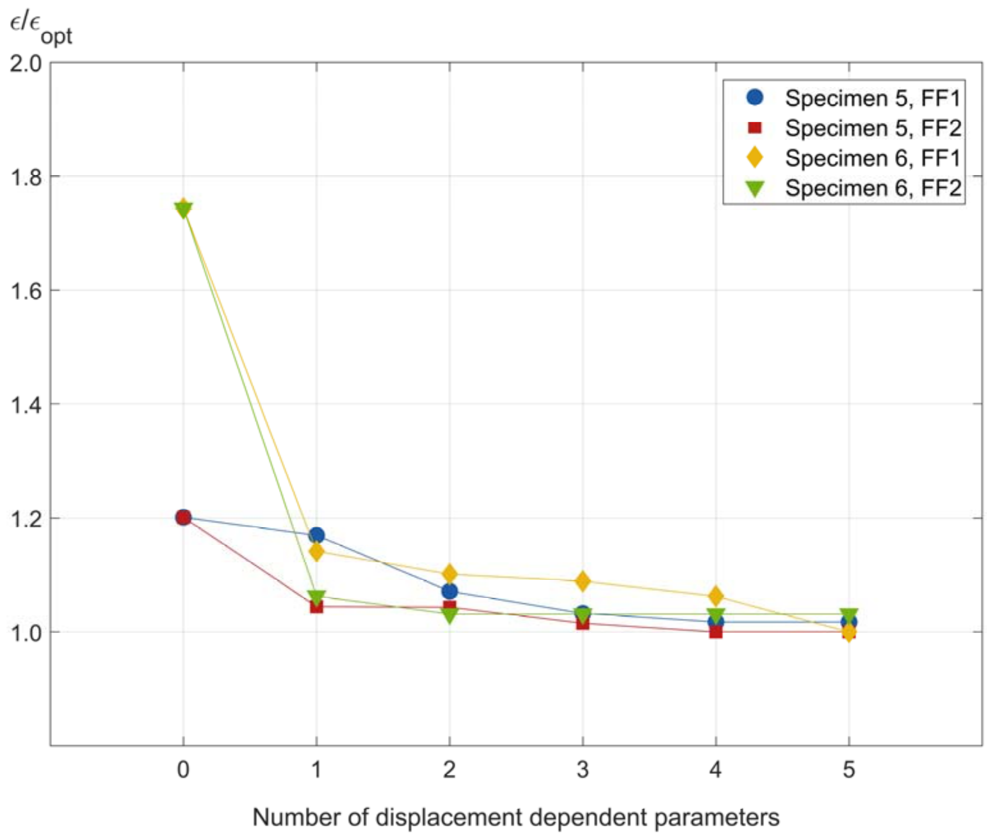

Figure 18. Relative error as a function of the number of displacement-dependent parameters for both specimens being calibrated with earthquake simulator tests.

SUMMARY AND CONCLUSIONS

A new simplified and versatile practitioner-oriented element model for seismic isolation elastomeric bearings has been presented. Its ability to accurately represent the behavior of different types of elastomeric isolators was demonstrated through the calibration of six different specimens, four with cyclic test results and two with earthquake simulation test results. The agreement between the experimental test data and the model-predicted values is entirely satisfactory for practical design purposes, even if most of the model parameters are displacement-independent, i.e., parameters that are not defined as a function of the isolator shear strain.

The calibration with cyclic tests was performed by minimizing different measures of error between test-measured and model-predicted values. The difference between dissipated energy, force history, and stiffness history for a deformation cycle were considered. Results showed that for isolators that exhibit significant hardening, the minimization of the force deviation delivers more robust optimal parameters than the minimization of the lateral stiffness error. This is the case because in minimizing the difference in lateral stiffness, the optimization procedure has a bias to the hardening region, allowing larger errors in the region of smaller stiffnesses, which are actually more likely to produce larger displacement increments.

For the earthquake simulation test calibration, two different functional forms were analyzed to constrain the variation of some of the parameters with the level of shear strain imposed in the isolator. Results showed that for the specimens that were considered, both functional forms led to similar error levels. Consequently, the use of a simple linear functional form (FF2) is recommended.

The proposed model can capture the hardening effect on elastomeric isolators accurately. Also, the type of isolator being modeled can be easily changed by modifying the six parameters of the model. Then, this novel model presents a highly desirable balance between accuracy and simplicity on its calibration. It can be readily implemented in academic or commercial software packages as the constitutive equations and the rules for unloading and reloading are presented in detail in this manuscript.

We recommend that manufacturers of commercial seismic isolators try to relate the bearings' geometric and material characteristics with the presented model's parameters. As seismic design codes require cyclic testing of isolator prototypes for each project, the model parameters can always be identified using real data. However, Tables 5, 6, 8, and 9 can serve as useful references for choosing optimal parameter values in an initial phase of the seismic isolation design.

In the last three decades, manufacturers have performed thousands of qualification, prototype, and production tests; consequently, they have gathered a vast quantity of proprietary test results. Manufacturers could use the model presented in this article and provide their customers the parameters required to reproduce the hysteretic behavior of their products. The availability of such data could facilitate the incorporation and evaluation of their products in the analyses conducted by structural engineers designing the isolation systems in specific projects.

ACKNOWLEDGMENTS

This research was funded by CONICYT Doctorado Nacional 21161027, the National Research Center for Integrated Natural Disaster Management CONICYT /FONDAP/15110017, and FONDECYT grant 1170836 (SIBER-RISK). The authors also would like to thank the John A. Blume Earthquake Engineering Center at Stanford University for hosting the first author during his one-year stay at Stanford as visiting student researcher and to Professor Masaru Kikuchi and Dr. Ian Aiken, who generously provided results of cyclic and earthquake simulation tests, used to calibrate the model presented in this article.

REFERENCES

Abe, M., Yoshida, J., and Fujino, Y., 2004. Multiaxial behaviors of laminated rubber bearings and their modeling. II: Modeling. *Journal of Structural Engineering*, **130(8)**, 1133-1144.

Bauschinger, J., 1881. Ueber die Veränderung der Elasticitätsgrenze und des Elasticitätsmoduls verschiedener Metalle. Civiling NF, **27 (19)**, pp. 289-348.

Bosco, M., Ferrara, E., Ghersi, A., Marino, E. M., and Rossi, P. P., 2016. Improvement of the model proposed by Menegotto and Pinto for steel. *Engineering Structures*, **124**, 442-456.

Bouc, R., 1971. A mathematical model for hysteresis. *Acta Acustica united with Acustica*, **24(1)**, 16-25.

Box, G. E., Luceño, A., and Del Carmen Paniagua-Quinones, M. (2011). *Statistical control by monitoring and adjustment*, Second edition, John Wiley & Sons.

Ciampi, V., Eligehausen, R., Bertero, V. V., and Popov, E. P., 1982. Analytical model for concrete anchorages of reinforcing bars under generalized excitations. Berkeley, CA, USA: College of Engineering, University of California.

Chen, M. C., Pantoli, E., Wang, X., Astroza, R., Ebrahimian, H., Mintz, S., Hutchinson, T., Conte, J., Restrepo, J., Meacham, B., Kim, J., and Park, H., 2013a. BNCS Report #1: Full-Scale Structural and Nonstructural Building System Performance during Earthquakes and PostEarthquake Fire - Specimen Design, Construction and Test Protocol, Structural Systems Research Project Report Series, SSRP 13/9, University of California San Diego, La Jolla, CA.

Chen, M. C., Pantoli, E., Wang, X., Mintz, S., Hutchinson, T., and Restrepo, J., 2013b. BNCS Report #4: Full-Scale Structural and Nonstructural Building System Performance during Earthquakes and Post-Earthquake Fire – Construction Details and Technical Specifications of Specific Subsystems, Structural Systems Research Project Report Series, SSRP 13/12, University of California San Diego, La Jolla, CA.

Dall'Asta, A., and Ragni, L., 2006. Experimental tests and analytical model of high damping rubber dissipating devices. *Engineering Structures*, **28(13)**, 1874-1884.

De la Llera, J.C., Luders, C., Leigh, P. and Sady, H., 2004. Analysis, testing, and implementation of seismic isolation of buildings in Chile. *Earthquake Engineering and Structural Dynamics*, **33(5),** 543–574.

Hwang, J. S., Wu, J. D., Pan, T. C., and Yang, G., 2002. A mathematical hysteretic model for elastomeric isolation bearings. *Earthquake Engineering & Structural Dynamics*, **31(4)**, 771-789.

Ibarra, L. F., Medina, R. A., and Krawinkler, H., 2005. Hysteretic models that incorporate strength and stiffness deterioration. *Earthquake engineering & structural dynamics*, **34(12)**, 1489-1511.

Lion, A., 1997. On the large displacement behaviour of reinforced rubber at different temperatures. *Journal of the Mechanics and Physics of Solids*, **45(11-12)**, 1805-1834

Kikuchi, M., and Aiken, I. D., 1997. An analytical hysteresis model for elastomeric seismic isolation bearings. *Earthquake engineering & structural dynamics*, **26(2)**, 215-231.

MATLAB 2020a, The MathWorks Inc. Optimization Toolbox. Natick, Massachusetts, United States; 2020.

Menegotto M, and Pinto PE., 1973. Method of analysis for cyclically loaded reinforced concrete plane frames including changes in geometry and non-elastic behaviour of elements under combined normal force and bending. IABSE symposium of resistance and ultimate deformability of structures acted on by well-defined repeated loads, vol. 13. Lisbon, Portugal: International Association of Bridge and Structural Engineering; 1973. p. 15–22.

Mullins, L., 1969. Softening of rubber by displacement. *Rubber chemistry and technology*, **42(1)**, 339-362.

Ramberg W, and Osgood WR., 1943 Description of stress-strain curves by three parameters Technical note No. 902. Washington DC: National Advisory Committee for Aeronautics; 1943.

Ozdemir, Non-linear transient dynamic analysis of yielding structures, Ph.D. Dissertation, Division of Structural Engineering and Structural Mechanics, Department of Civil Engineering, University of California, Berkeley, 1976.

Pan, T. C., and Yang, G. (1996, June). Non-linear analysis of base-isolated MDOF structures. *In Proceedings of the 11th World Conference on Earthquake Engineering, Mexico.*

Tsai, C. S., Chiang, T. C., Chen, B. J., and Lin, S. B., 2003. An advanced analytical model for high damping rubber bearings. *Earthquake engineering & structural dynamics*, **32(9)**, 1373-1387

Tsopelas, P., Constantinou, M. C., and Reinhorn, A. M. (1994). 3D-BASIS-ME: Computer program for non-linear dynamic analysis of seismically isolated single and multiple structures and liquid storage tanks.

Tubaldi, E., Ragni, L., Dall'Asta, A., Ahmadi, H., and Muhr, A. (2017). Stress softening behaviour of HDNR bearings: modelling and influence on the seismic response of isolated structures. *Earthquake Engineering & Structural Dynamics*, **46(12)**, 2033-2054.

Wen, Y. X., 1976. Method for random vibration of hysteretic systems. *Journal of the engineering mechanics division*, **102(2)**, 249-263.